MECHANICAL CHARACTERIZATION OF HYBRID MATERIAL SYSTEMS CONSISTING OF SHEET METAL AND ADVANCED COMPOSITES

Michael Dlugosch[1], Dirk Lukaszewicz[2], Jens Fritsch[1] and Stefan Hiermaier[1]

[1]Department of Material Dynamics, Fraunhofer Ernst-Mach-Institute, EMI
Eckerstraße 4, 79104 Freiburg, Germany
Email: Michael.Dlugosch@emi.fraunhofer.de , web page: http://www.emi.fraunhofer.de/
Email : Jens.Fritsch@emi.fraunhofer.de
Email : Stefan.Hiermaier@emi.fraunhofer.de

[2]Department of Passive Safety, BMW Group
Knorrstraße 147, 80788 Munich, Germany
Email: Dirk.Lukaszewicz@bmw.de , web page: http://www.bmw.de

Keywords: Hybrid materials, Experimental characterization, Coupon testing, Automotive crash structures

ABSTRACT

Strip-shaped hybrid coupon specimens comprised of steel and glass/carbon fiber reinforced plastics are tested under quasistatic tension and 3-point-bending. The effects of major material and design parameters (steel and fiber type, laminate thickness and layup) on the stiffness, strength and the specific energy absorption are assessed. Furthermore, hybrid mechanisms resulting from the mutual interaction of both constituent materials are presented. Although anticipated effects on the hybrid specimens' stiffness and strength are widely confirmed, the fiber type for example exhibits a distinctly smaller impact than expected. The specimens' loading and failure behavior is rather dominated by the type of steel and its characteristics. Thus, glass fiber reinforced hybrid variants generally keep up with carbon fiber reinforced hybrid variants in terms of mechanical properties. Considering the difference in price, this is of particular interest for hybrid mid or high volume crash structural applications. As hybrid mechanism, a distinct extension of the maximum strain is observed for both composites (up to 48 %) and steel (up to 23 %) when joined in a hybrid specimen and tested under tensile loads. Furthermore, having composites on the rather pressure loaded side in 3-point-bending results in a 26 %-increase in mass specific energy absorption (compared to reverse loading) due to an enhanced composite failure mode and the stabilizing effect of the steel strip.

1 INTRODUCTION

Weight reduction plays an increasingly important role in many engineering disciplines such as automotive or aircraft engineering. This is motivated by a number of factors including efficiency goals and more strict regulations for CO_2 emissions for European car manufacturers in 2020 [1]. Different lightweight design strategies (e.g. material or integrative lightweight design) have been developed in the last decades [2], which – in order to achieve the highest weight savings possible – best be combined in a synergetic manner. Pursuing comprehensive lightweight design thus means developing highly integrated structures that are made of lightweight materials such as advanced composites and that are optimized in shape to efficiently fit all loading requirements.

In accordance with an increasing complexity of requirements for engineering structures, especially in crash applications, the latest developments in research concerning lightweight materials identified so called hybrid systems as one very promising way to realize advanced lightweight structures rather than one single "best" material [3, 4]. Hybrid material systems consist of two or more materials or material systems such as advanced composites and can be arranged in a multitude of architectural designs. Consequently, it is possible to answer a complex set of requirement specifications with a corresponding

set of features inherent in a specifically designed hybrid structure combining completely different types of materials and their properties. Since it predefines possible load paths and thus enables the exploitation of the materials' full potential, the shape of the hybrid structure is just as important as the selection of combined materials. Advanced composites in this context are considered polymer matrix materials reinforced with carbon- (CFRP) or glass-fibers (GFRP).

In order to design such hybrid structures for crash applications, it is necessary to understand the behavior not only of the single basic materials but also the mechanisms and interactions of the constituents as well as the interfaces or joints.

Research on the mechanical behavior of hybrid material systems consisting of advanced composites and metals so far mostly originated from direct applications in complex engineering systems rather than in the field of fundamental material research. In the 1990s Ford produced a high volume vehicle with a hybrid front end structure composed of a sheet steel framework and injection molded rib reinforcements of glass fiber reinforced polyamide [5]. Next to weight specific increases in strength and stiffness they discovered high integrative potential and good recyclability. Further investigations on hybrid structural automotive components like b-pillars, door sills and roof or floor structures have been conducted by several authors [6–10]. These investigations were often embedded in industry-oriented research projects that resulted in case and feasibility studies concerning direct applications of hybrid structures with respect to weight savings, production techniques and costs. As a general result, those hybrid structures could be identified as feasible solutions in the respective fields of application with the possibility of moderate to high weight savings, higher integration levels and/or enhanced mechanical properties compared to conventional solutions.

Focusing on the mechanics and the crashworthiness of hybrid structures in automotive crash applications Costas et al. [11] investigated front crash absorbers that comprise of steel tubes with various core inserts such as CFRP, GFRP or polyethylene foam. All types of inserts showed a different crash behavior according to their individual geometric shape. Wang et al. [12] conducted quasi static and dynamic impact tests on steel cylinders circumferentially wrapped with GFRP and found the composite material to be an effective reinforcement to the tubes. According to their results the strengthening effect grew with an increasing composite to steel ratio, eventually leading to an altered, more effective failure mode. Disadvantageous changes in the failure mode were observed by Bouchet et al. [13] while crushing aluminum cylinders circumferentially wrapped with GFRP. A dependency on the thickness of the tube as well as on the composite reinforcement was found, but no correlation to any sort of surface treatment at the bonding interface. Similar findings were made by Shin et al. [14] wrapping GFRP prepregs around square aluminum tubes. In quasi static crushing tests they discovered a specific reinforcing effect of GFRP depending on the ply orientations and the composite thickness. Kim at al. [15] also studied the crashworthiness of aluminum square tubes reinforced with CFRP subjected to axial low velocity impact. They found that CFRP reinforcements enhanced both the CFE (crush force efficiency) and the *SEA* (weight specific crash energy absorption capability) of the crush tubes by 30 % and 38 % respectively. Related studies were conducted by Bambach et al. [16–22]. The authors analyzed the reinforcing effect of externally applied CFRP on crush tubes of different specifications. The influences of the tube design and material as well as the number and orientation of the CFRP layers on the crash characteristics were investigated. They found substantial improvements in crash performance compared to tubes made of one single material (Mamalis [23]). However, the impact characteristics of composite crush tubes strongly depend on the complex failure mechanisms within the material [24] and thus have a vast range of values for their metrics of crashworthiness such as the CFE ("crush force efficiency") or *SEA* ("specific energy absorption"). Considering other factors such as geometric, bonding or architectural aspects a direct comparison between the different materiel systems is difficult. The abovementioned scientific publications indicate significant weight saving potentials inherent in hybrid materials comprised of fiber reinforced plastics and metals. They also indicate their strong dependency on their architectural design and single material constituents. Thus, the conclusions drawn from the test results can only be valid for the respective set of parameters (e.g. specimen geometry) and can hardly be transferred to other settings or even be generalized.

Basic mechanical characterization of hybrid material systems studying flat coupons under tension and bending has mainly been conducted in the context of FMLs (fiber-metal-laminates) [25]. FMLs

generally show superior characteristics to other material systems under impact loading and concerning fatigue strength, but represent custom-built solutions for specific applications in the aerospace sector. A slightly more general analysis has been published by Uriayer [26], who tested CFRP laminates sandwiched between two strips of steel sheets under tension and found a bilinear response in the stress strain behavior of the specimens due to reaching of the steel's yield stress before the maximum stress of the CFRP. After the fracture of the CFRP component the specimens exhibited a ductile behavior of the still intact steel strips until total failure.

A rather comprehensive study of hybrid materials on a coupon level was conducted by Mildner [27]. Specimens composed of aluminum or steel adhesively bonded to GFRP- or CFRP-laminates of different fiber layups were tested under quasistatic tension and 3-point-bending conditions. Although the vast majority of tension tests had to be aborted directly after the laminate fracture due to the failure of the clamping mechanism, several interesting observations were made. According to predictions based on rule-of-mixture calulations for non-unidirectional fiber orientations in the laminates the stiffness of hybrid specimens did not reach the levels of pure steel. The hybrids' stress-strain-curve also showed a bilinear behavior except for unidirectional CFRP-steel specimens, which reached laminate fracture before reaching the yield stress of the steel. Hybrid specimens with laminates with mostly longitudinal (0°) fiber orientations outperformed pure steel specimens in terms of strength while predominantly transversally reinforced hybrid specimens did not.

The aim of this study is to establish a systematic approach to the mechanical characterization of hybrid material systems consisting of advanced composites and metals and to extend the scientific foundation in this area of research on hybrid materials. The central idea is to identify basic principles that determine the qualitative mechanical behavior of those hybrid systems up to failure such as the rule-of-mixtures or the effects of major design parameters. A second goal of this study was to fundamentally assess the potential of different hybrid systems for the application in automotive structures particularly subjected to crash loads.

Hybrid specimens consisting of sheet metals adhesively bonded to advanced composite laminates were tested in bending and tension up to failure under quasi-static conditions. In order to isolate the material effects and to rule out geometric or architectural factors flat coupon specimens were chosen in this study.

2 MANUFACTURING OF THE SPECIMENS

2.1 Selection of materials

Metals – With the aim of qualifying hybrid material systems for automotive lightweight structures subject to crash loads the selection of materials referred to materials already used for crash relevant structures in current vehicle designs. As a result of crash load cases such as the frontal or side impact and architectural vehicle design, different materials have found application in defined areas of the BiW (body-in-white) to meet specific requirements. As indicated in Figure 1 the front of the vehicle represents a deformation zone with mainly dual-phase (yellow) steels able to absorb crash energy while folding in a stable manner during a front crash.

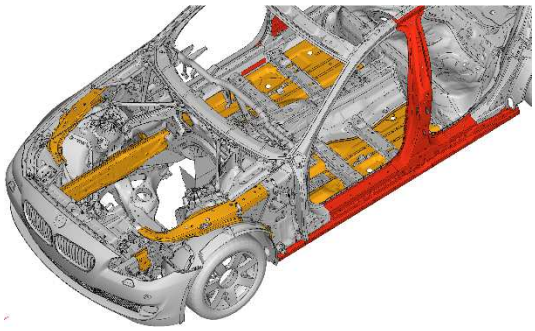

Figure 1: Applications of dual-phase and press hardened steel in current vehicle BiWs.

The side structures in contrast do not allow for major deformations since intrusions into the passenger compartment need to be minimized. Therefore, the side of current vehicle BiWs is dominated by very stiff structures often comprised of press hardened steel (red) mainly because of its increased yield strength. In order to represent those entirely different types of steel commonly used in the BiW design a dual phase steel named “HCT600X+Z100“ [28] and hardened boron-steel named “22MnB5” [29] were used for the manufacturing of the test specimen. Both steels are abbreviated as “HCT” and “MnB” respectively below.

Composites - The fiber reinforced plastics (FRPs) were chosen with respect to their potential automotive application. Key factors for the material selection were thus the anticipated mechanical performance, the manufacturability and costs. The composite layups were manufactured using semi-manufactured products (prepregs) consisting of unidirectional glass or carbon fiber mats pre-impregnated with epoxy resin. Both the carbon fiber prepreg “PREDO PR-UD CS 300/600 FT 102 38” [30] and the glass fiber prepreg “PREDO PR-UD EST 300/300 FT 102 35” [31] were produced by SGL epo GmbH. To ensure comparability both prepregs contained the same epoxy resin matrix “FT102” [32] and had a fiber areal weight of 300 g/m^2. The fiber volume fractions were 62 % and 65 % for the carbon and the glass fiber prepreg respectively. The types of reinforcing fibers used in this study were 50k filaments industrial grade carbon fibers and standard E-glass fibers, which are commonly used in engineering applications such as automotive or aircraft systems.

Adhesive - Joining of the constituents was achieved through a layer of “BETAMATE 2096” [33], a two-component epoxy structural adhesive widely used in the automotive sector for crash, structural and repair applications. This type of adhesive has proven to be suitable for joining composites and metals in previous test series [34].

2.2. Specimen design

For the 3-point-bending and tension tests, simple flat coupon specimens were designed as a two-layer thin plate consisting of a steel sheet of 1.5 mm constant thickness adhesively bonded to a cured layup of composite prepregs. As to be seen in Figure 2 and Table 1, the dimensions of the specimens were 190 mm in length, 15 mm in width with a varying total thickness in the range of 2.8 mm – 6.8 mm depending on the layup type.

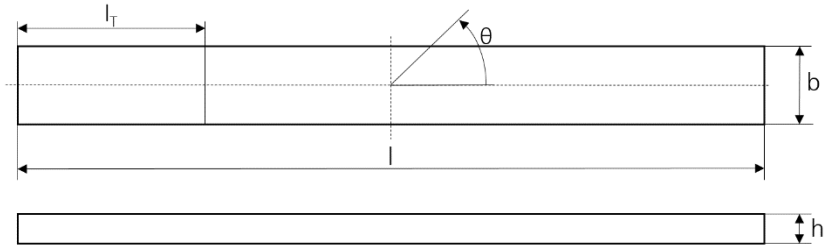

Figure 2: Specimen design for the tension and 3-point-bending tests

Parameter	Description	Level(s)		
l	Total length	190 mm		
b	Width	15 mm		
h	Total thickness	Number of plies	GFRP	CFRP
		4	2.8 mm	3.1 mm
		8	3.6 mm	4.6 mm
		16	5.9 mm	6.8 mm
l_T	Clamping / support length	Tension		45 mm
		3-Point-Bending		25 mm
θ	Fiber angles (0° indicates the specimen’s length axis)	0°, 45°, 90°, 135° (≙ -45°)		

Table 1: Specimen parameters and their levels

The parameters varied in this study were the types of steel and reinforcing fibers, the fiber or ply orientations as well as the thickness of the composite layups within the hybrid specimen. Table 2 shows the full list of the parameters of variation and their levels.

Type of steel	Type of fibers	Layup orientations	Number of plies
HCT600X +Z100	SGL 50k carbon fiber	[0°/90°]	4
22MnB5	PPG E-glass fiber	[±45°]	8
		Isotropic [0°/±45°/90°]	16

Table 2: Parameters of variation for the test program

Considering the parameters of variation and their levels, a full factorial design of the testing variants' matrix leads to 36 variants total. Thus, a systematic selection of variants from the full factorial design plan was made in order to determine main effects of the parameters of variation and reduce the variant matrix to a reasonable size of 22. The reduced list of testing variants was set up by defining standard parameter levels and periodic sampling points in the design space covering all major parameter levels.

2.3 Manufacturing

The manufacturing process of the specimens can be subdivided into several consecutive steps. The different composite laminates were produced manually by stacking the prepregs according to the predefined layups (numbers and orientations of the plies). After that, the laminates were cured in an autoclave at a heating/cooling rate of 4 K/min and maximum pressure and temperature levels of 3 bar und 140 °C respectively with a dwell time of 3.5 hours. To prepare the steel parts for bonding they were sandblasted before cleaning them with acetone. A thin layer of BETAMATE 2096, a two component epoxy structural adhesive was applied to the whole surface with a spatula. Then, the two constituents were joined in a press and left for at least 48 hours at room temperature to guarantee a minimum curing ratio of 90 % of the epoxy adhesive before shipping. The tension and bending test specimens were extracted at specifically defined random locations of the hybrid plates by a high precision water-jet-cutting-machine.

3 TESTING AND EVALUATION PROCEDURES

All experiments were conducted on an Instron servohydraulic universal testing machine as schematically depicted in Figure 3. A load cell with a piezo-electric-force-sensor (range up to 100 kN) provided a force-time-signal with a data recording rate of 100 Hz. The transient recorder as part of the servohydraulic moving piston provided a position-time-signal to be processed into a strain output. Due to a limited stiffness of the testing machine and partly high loads during the experiments a load-dependent error was imposed on the results, which was corrected on the base of previous analyses before further data evaluation.

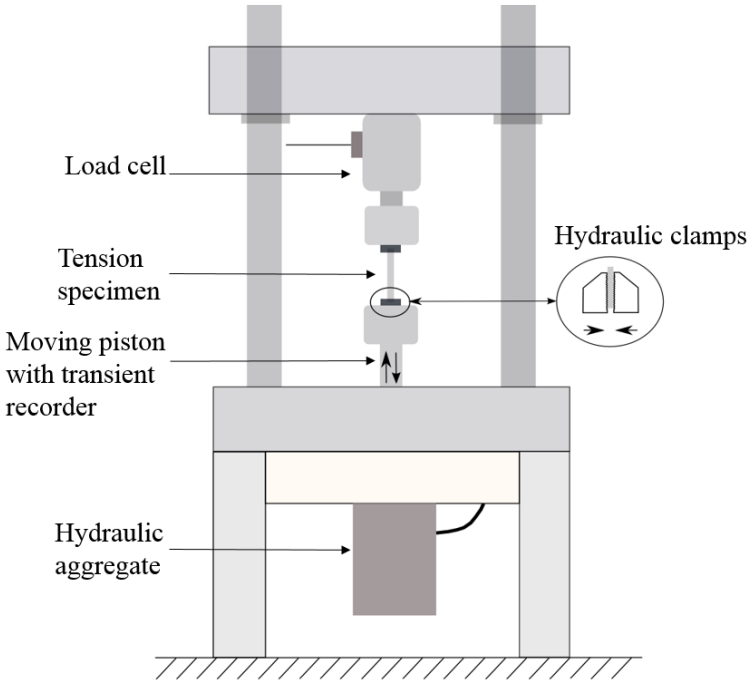

Figure 3: Schematic depiction of the Instron servohydraulic testing machine.

The constant loading velocity was adjusted individually to the free length between the clamps to assure a constant technical strain rate of 0.01 1/s for the tension tests. The same velocity of 1 mm/s was set for the bending tests. In order to assure statistic robustness, at least four valid experiments (consistent load levels and failure modes) per variant were conducted. All experiments were carried out at standard testing climate conditions (23 °C, 50 % humidity).

3.1 Tensile tests

All tensile tests were conducted until total failure of the specimens and full separation of both clamped ends. The hydraulic clamping pressure of 200 bar was held constant for the entire duration of the experiments. Additional cap strips were not required since no slipping occurred and failure was rarely initiated within the clamps. High speed cameras were applied to additionally perform optical strain measurements via digital image correlation (software: ARAMIS by GOM [35]) for one experiment of each variant to compute a scaling factor for the machine data.

3.2 Bending tests

The 3-point-bending tests were conducted using a setup with two supports and one fin - all with a radius of 5 mm. The supports had a distance of 140 mm as depicted in Figure 4.

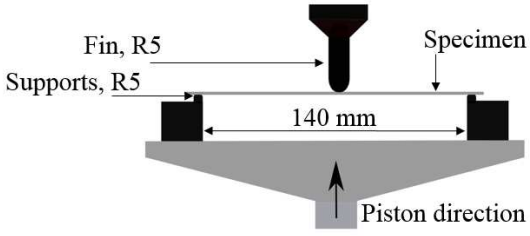

Figure 4: Test setup for the 3-point-bending tests

In contrast to the tensile experiments, the bending tests had a fixed maximum piston displacement of 40 mm independent of the specimen failure. Also, due to much lower forces and thus negligible

systematic machine compliance error, the transient recorder signal could be assessed directly as piston and support displacement.

3.3 Evaluation of results and mechanical characteristics

Qualitative behavior – In order to qualitatively assess the performance of the hybrid specimens, force-displacement- or force-strain-diagrams were analyzed. Due to the consecutive failure of the two phases within a hybrid specimen a sudden change of its cross-sectional area led to an abrupt increase in the stress signal, which complicates intuitive interpretation.

Stiffness – Since there is no standardized method for the stiffness evaluation for hybrid materials, the standard for the tensile characterization of fiber reinforced plastics DIN EN ISO 527-4 [36] was taken as a guideline for tensile tests. The slope of a linear fit to the stress-strain-curve in the linear elastic regime of the specimen was interpreted the stiffness value. For bending tests the stiffness *E* was assessed according to the respective standard for FRPs DIN EN ISO 14125 [37] with equation (1) as

$$E = \frac{l_0^3 \Delta F}{4 \cdot \Delta s \cdot b \cdot t^3}\ , \tag{1}$$

with l_0 representing the free length of the specimen between the supports, ΔF and Δs as the differences in the force signal and the outer fiber strain at the standardized measurement points as well as *b* and *t* as the specimen's width and thickness.

Strength – The strength of a hybrid specimen was defined by the maximum stress it can withstand before failure of any kind is observed. With the FRPs generally featuring a relatively low maximum strain compared to metals, the first FRP failure marked the beginning of the hybrid specimen failure. Thus, the maximum technical stress was normally observed at the point of FRP-fracture. The strength value for the tensile tests was defined as the maximum technical stress, hence the maximum force in relation to the specimen's original cross-sectional area. For the maximum bending strength σ_{max}, equation (2) according to

$$\sigma_{max} = \frac{3}{2}\frac{F_{max} \cdot l_0}{b \cdot t^2} \tag{2}$$

was solved with F_{max} representing the maximum force as defined in the FRP standard.

Specific Energy Absorption (SEA) – The *SEA* is a typical crashworthiness metric and was exclusively assessed for the bending tests. It relates the energy absorbed during loading and failure to the specimen's mass *m* as in equation (3)

$$SEA = \frac{1}{m} \cdot \int F(x)\ . \tag{3}$$

The absorbed energy equals the integrated force *F* over the displacement and can be interpreted as the area underneath a force-displacement-plot.

Hybrid mechanisms – Findings introduced as "hybrid mechanisms" represent effects that are particularly specific for the hybrid material systems tested in this study. These mechanisms develop due to the specific interaction of advanced composites and steel sheets and can hardly be anticipated considering the mechanical behavior of the two basic constituents separately.

4 RESULTS

The following results are structured according to the load case and the mechanical characteristics named above. For obvious reasons, the entire scope of results cannot be presented in this paper. Hence, a selection of the major results and findings is introduced below.

4.1 Tension tests

Qualitative behavior – A typical force-strain-diagram of a hybrid specimen (green) as depicted in Figure 5 illustrates the qualitative behavior compared to a pure HCT (gray) and CFRP (blue) specimen. The force-strain-curve of the hybrid specimen shows a bilinear behavior under tension loading as to be

seen in the right graph of Figure 5 showing a zoomed view of the diagram on the left. The kink in the force-strain-curve of the hybrid specimen coincides with the elastic limit of the pure steel specimen suggesting an “elastic-plastic-behavior” of the hybrid specimen under tension.

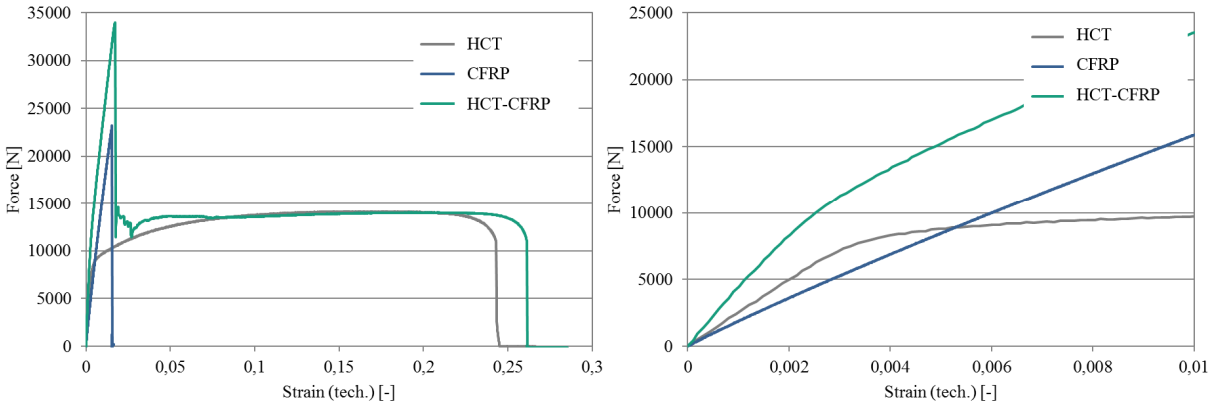

Figure 5: Force-strain-curves of pure steel (HCT), CFRP and hybrid specimens under tension
Parameters: HCT, CFRP, 8 plies, [0°/90°]-layup

While pure CFRP shows a linear force-strain-curve until abrupt brittle fracture, the hybrid specimen resembles a cumulative curve of the pure steel and the pure CFRP specimens’ behavior. Consequently, the hybrid force-strain-curve adapts to the load level of the pure steel specimen after CFRP laminate fracture until necking and failure of the remaining steel phase.

Stiffness – According to analytic rule-of-mixture calculations for non-unidirectional GFRP and CFRP layups as well as experimental measurements pure FRP laminates feature a lower stiffness than steel. Thus, the tensile stiffness of the hybrid specimens is mainly dominated by the steel phase. As presented in Figure 6 the stiffness decreases with an increasing number of FRP plies confirming analytic calculations. The overall stiffness decreases with a rising cross-sectional share of the less stiff FRP-phase.

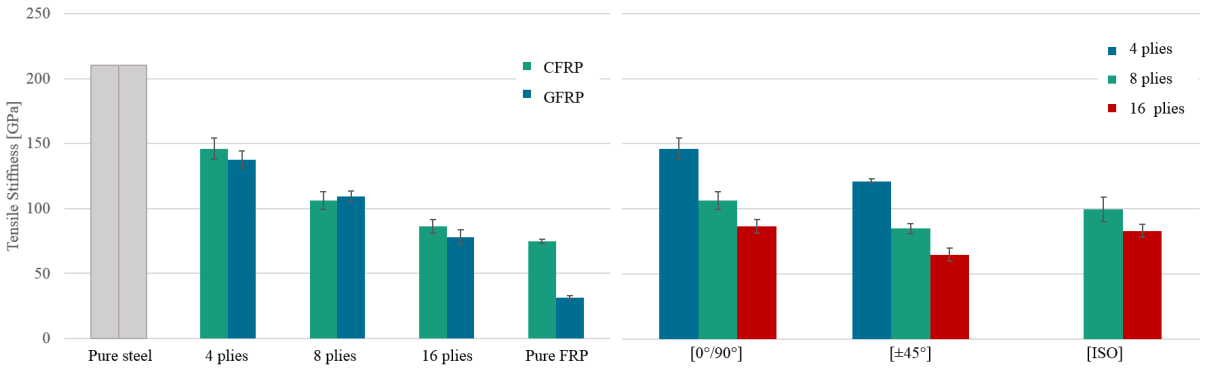

Figure 6: Tensile stiffness of pure steel, hybrid and pure FRP specimen
Parameters: HCT, [0°/90°]-layup (left) / HCT, CFRP (right)

The diagram on the left in Figure 6 illustrates, that the fiber type does not significantly affect the stiffness of a hybrid specimen. A distinct difference between the stiffer carbon fiber and the less stiff glass fiber is observed for pure FRP specimens, which confirms the conclusion, that the stiffness is mainly dominated by the steel phase of the hybrid specimens. As depicted in the right graph in Figure 6, the decrease of stiffness with an increasing cross-sectional share of FRP is independent of the layup. Furthermore, the tensile stiffness of hybrid specimens is proportional to the amount of fibers in the 0°-direction, as it constantly rises from [±45°]- to [ISO]- to [0°/90°]-layups.

Strength – Rather similar findings are made concerning the tensile strength of hybrid materials.

While the type of reinforcing fibers (not pictured here) and the number of FRP plies don't significantly affect the specimens' strength, the type of steel shows a clear impact as depicted in the right graph of Figure 7.

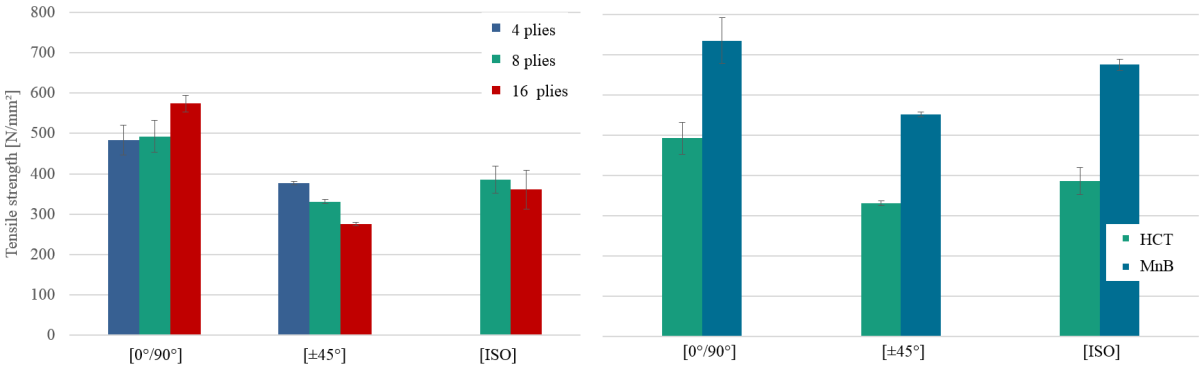

Figure 7: Tensile strength with respect to fiber layup, number of plies and type of steel
Parameters: HCT, CFRP (left) / CFRP, 8 plies (right)

This indicates that the strength of the hybrid specimens is dominated by the type of steel and its particular strength. Both graphs in Figure 7 show, that the fiber layup has a similar effect on the strength as on the stiffness, as the specimens' strength increases with an increasing amount of fibers oriented in the 0°-direction. The measured strength values for the pure constituent materials are 637 N/mm^2 and 1454 N/mm^2 for HCT and MnB as well as 411 N/mm^2 and 512 N/mm^2 for GFRP and CFRP respectively.

Hybrid mechanism – One hybrid mechanism observed during tensile testing is the extension of the maximum strain to failure for the individual constituents when combined in a hybrid specimen. This is particularly distinct for specimens comprised of press hardened steel (MnB) and GFRP as depicted in Figure 8.

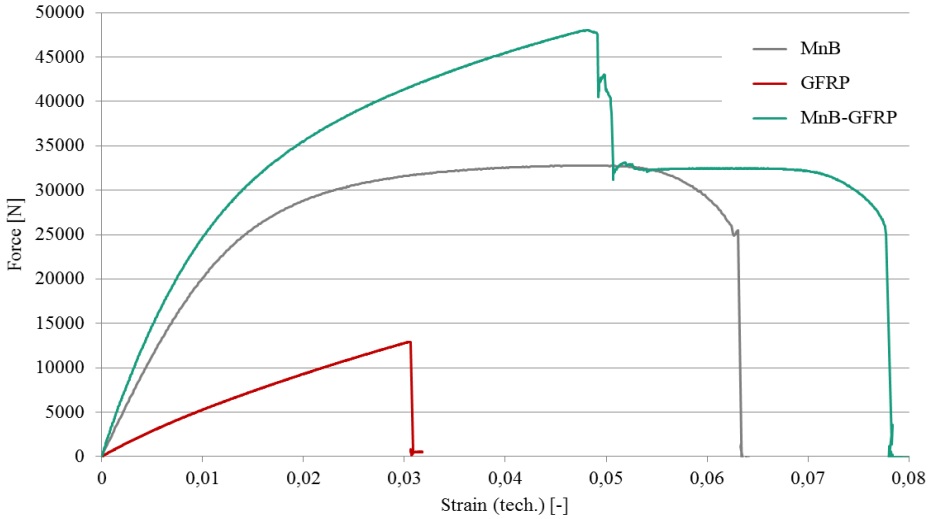

Figure 8: Force-strain-plots of a hybrid MnB-GFRP-specimen and its individual constituents
Parameters: MnB, GFRP, 8 plies, [0°/90°]-layup

After laminate fracture in the hybrid specimen (green) the force level remains on the level of the pure steel specimen with an extended maximum strain of approximately 120 % that of the pure steel specimen. While the effect seems independent of the type of reinforcing fiber, there is a distinct difference between the types of steel as shown in Table 3. When comparing the strain to failure of the pure GFRP specimen with the strain to failure of the GFRP-phase of the hybrid specimen, it becomes evident, that also the strain to failure of the FRPs is affected by the hybridization with steel.

	Strain to failure [-] Pure material specimen	Strain to failure [-] Within hybrid specimen	Ratio [%] Hybrid/Pure material
MnB	0.06	0.07	123
HCT	0.24	0.23	94
CFRP	0.02	0.026	128
GFRP	0.03	0.04	148

Table 3: Strain to failure mean values for pure material and hybrid specimens

Table 3 shows that a hybridization with FRPs extends the strain to failure for press hardened steel by approximately 23 % and reduces the measure for dual phase steel by mere 6 % (not significant regarding the standard deviation). The strains to failure (laminate fracture) of CFRP and GFRP are extended by 28 % and 48 % respectively. While ongoing research is determining the underlying mechanisms in detail, a first theory is presented here. Due to the constraining effect of the FRP on the steel phase of the hybrid specimen, lateral strains are constrained during tensile tests causing stresses in the 90°-direction. According to the forming limit curve (FLC) [38] additional stresses in the lateral direction cause an elevated forming limit (e.g. increased strain to failure) in the longitudinal 0°-direction for steel specimens under tension. The contrary effect between both types of steel is a matter of ongoing research. Kumazawa and Takatoya [39] tested cruciform CFRP-specimens under biaxial tension and found an increase in the maximum longitudinal strain when additionally applying a negative stress in the lateral direction. Further experiments proved the comparability to strip-shaped uniaxial tension specimens. Thus, a mutual effect could take place within the hybrid specimens. The lateral contraction of the steel phase is constrained by the FRP laminate, causing lateral tension stresses in the steel phase and lateral pressure stresses in the FRP phase. Both stresses cause an extension of the maximum strain in the respective material phase. These findings need to be confirmed through further tests on pure GFRP and CFRP specimens of the laminates at hand.

4.2 Bending tests

Qualitative behavior - Figure **9** shows typical force-displacement-plots of pure steel, pure CFRP and hybrid 3-point-bending samples. Variants comprised of MnB and GFRP exhibit a fairly similar qualitative behavior. All of the hybrid specimens depicted in Figure **9** were tested with CFRP on the tension loaded side (facing the supports, see Figure 4). Stepwise laminate fracture is observed for pure CFRP and hybrid specimens. Laminate fracture is initiated in the lowermost ply as it is subjected to the highest outer fiber strain and progresses through the thickness of the laminate with a stepwise joint fracture of two to four plies at a time.

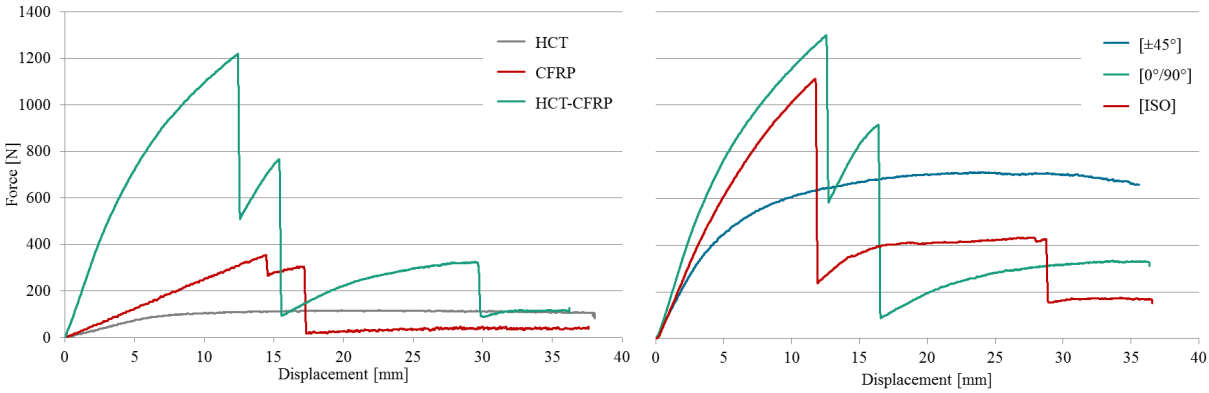

Figure 9: Force-displacement-plots of 3-point-bending tests
Parameters: HCT, CFRP, 8 plies, [0°/90°]-layup (left) / HCT, CFRP, 8 plies (right)

As depicted in the left graph of Figure **9** the maximum load of the hybrid exceeds the (imaginary)

cumulative curve of both constituent materials. This is due to geometrical effects, caused by the higher thickness of hybrid specimens and its effect on the bending stiffness. The left graph also shows, that neither of the specimens has entirely failed during the experiment with a predefined displacement and that the load level of the hybrid specimen adapts to the level of pure steel as seen before in the tension tests. The right graph in Figure 9 compares force-displacement-plots of hybrid specimens with different layups. According to the amount of fibers in the 0°-direction an isotropic layup generally produces a lower load level than a [0°/90°]-layup. While isotropic and [0°/90°]-layups fail in the above-mentioned stepwise manner, [±45°]-layups feature a rather smooth load-displacement-curve. The specimens with a [±45°] layup also exhibit only minor – if any – outer signs of laminate fracture after the bending test as depicted in Figure 10.

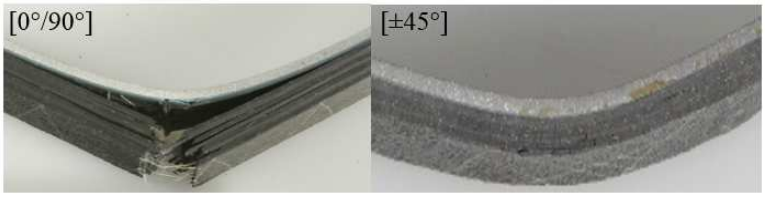

Figure 10: HCT-CFRP-hybrid specimens with [0°/90°] and [±45°] layups after 3-point-bending

Stiffness – The measured stiffness values of hybrid specimens (according to equation 1) widely confirm the anticipated effects of the parameters of variation. As shown in Figure 11, hybrid specimens with CFRP feature a significantly higher stiffness than those with GFRP, while hybrid specimens in general are less stiff than pure steel. For pure FRP variants the measured stiffness in relation to steel are 0.34 for CFRP and 0.11 for GFRP, which generally confirms the measurements from tensile tests.

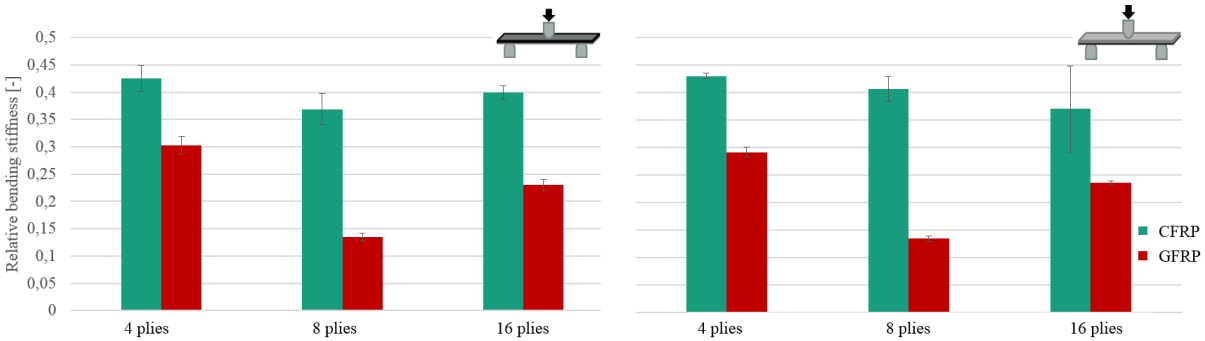

Figure 11: Bending stiffness relative to pure steel with reference to fiber type and number of plies
Parameters: HCT, [0°/90°]-layup

When comparing the left and the right diagram in Figure 11, it is evident, that the loading direction does not affect the bending stiffness. Since the stiffness is measured in an area of very small deflections, the different behavior of steel and FRP as the outer fiber is of small impact. Both diagrams show a dip in the stiffness with eight plies. This is due to two contrary effects of an increased hybridization. While the material stiffness decreases (as seen in the tension test results) the geometric stiffness simultaneously increases which creates a dip in the stiffness for variants with eight plies particularly significant for GFRP variants. Although those effects should be compensated through the stiffness calculation using equation (1), they prevail indicating the limits of applicability of the respective FRP-standard.

While Figure 11 only shows [0°/90°]-variants, the presented effects apply to the other layups as well. Also, the bending stiffness shows the same dependence on the fiber layup as the tensile stiffness – it is proportional to the amount of fibers in the 0°-direction. Thus, the bending stiffness in general seems predominantly affected by the fiber type and orientation.

Strength – The above-mentioned proportionality to the amount of fibers in 0°-direction is observed for the bending strength as well. Also, hybrid variants comprised of the press hardened steel excel the strength of those with HCT by 34 % on average. Figure 12 depicts the bending strength of hybrid

specimens of various ply numbers and both fiber types. Values of pure steel and FRP specimens are not pictured here, since failure was only partly reached and the differences in the respective failure mechanisms hinder a profound comparison.

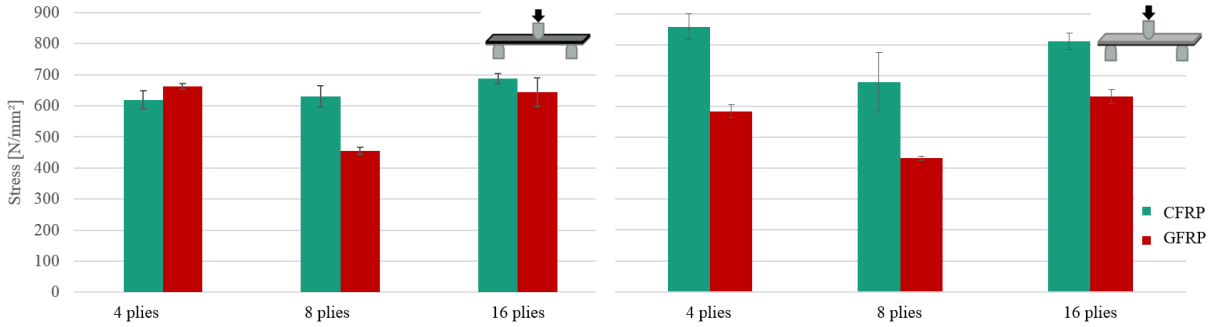

Figure 12: Bending strength of hybrid specimens with reference to the fiber type and the number of plies
Parameters: HCT, [0°/90°]-layup

Both graphs in Figure 12 show the superior strength of CFRP-variants over GFRP-variants. While GFRP-variants don't show any major dependence on the loading direction, hybrid CFRP-variants exhibit a higher strength when loaded with CFRP facing the supports. Generally the latter is to be expected since facing the supports, the fibers are mainly loaded under tension. Since the bending strength is also dominated by the steel type and glass fibers exhibit a tensile strength of around 50 % that of carbon fibers, the difference in loading direction with GFRP-variants does not translate into higher bending strengths.

Furthermore, both diagrams in Figure 12 show a dip in strength with eight plies. This is consistent with the stiffness results and is due to two contrary effects of an increased hybridization described above.

SEA – Due to the higher specific stiffness and strength of carbon fibers, the specific energy absorption trends to reach higher values for CFRP- than for GFRP-variants. This effect is more distinct for [±45°]-layups than for the [0°/90°]-layups pictured in Figure 13.

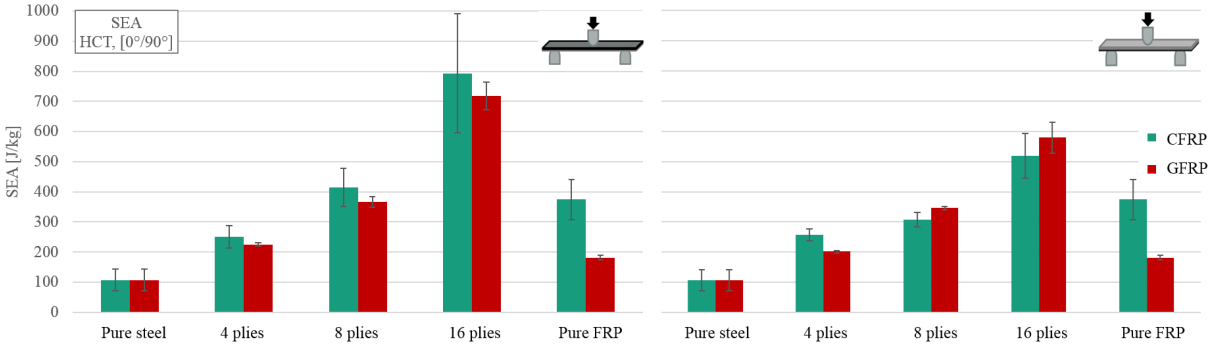

Figure 13: *SEA* with reference to the fiber type and the number of plies
Parameters: HCT, [0°/90°]-layup

While different fiber layups show volatile and rather insignificant effects on the *SEA*, the type of steel – as expected - has a crucial effect. Hybrid variants with MnB exhibit 34 % higher *SEA* values than HCT-variants on average. As depicted in Figure 13, the *SEA* increases clearly with a rising number of plies in the laminate. Although there is a significant increase in the geometric stiffness with thicker FRP-laminates, this effect is important for the evaluation for future applications as it still normalized to the specimen mass. This means, that the overall force level is enhanced with an increasing hybridization through the combination of a higher mass-specific geometric stiffness and a matching failure mechanism. Larger ranges of errors for CFRP-variants result from an observed higher probability of catastrophic failure like a collapse of the adhesive layer or extensive delaminations.

Hybrid mechanism – Under 3-point-bending one hybrid mechanism is the increased specific energy absorption with a loading direction having FRPs on the rather pressure-loaded side (facing the fin) of the specimen. While design guidelines for advanced composites recommend to have fibers loaded under tension, the amount of absorbed energy in 3-point-bending is generally higher with FRPs facing the fin, as depicted in Figure 13. The *SEA* values of the hybrid specimens in the left diagram are significantly higher than those in the right diagram (26 % on average). This effect is independent of all parameters of variation. As pictured in Figure 14, there is a fundamental difference in the failure mode between the two loading directions. Laminates facing the supports show a stepwise fracturing pattern as discussed above and pictured in lower left of Figure 14. Facing the fin, the laminates exhibit a mixed failure mode of fiber bending, fracture and delamination caused by mutual penetration of the fracture banks. These mechanisms are clearly visible in a through-thickness CT scan pictured on the right in Figure 14.

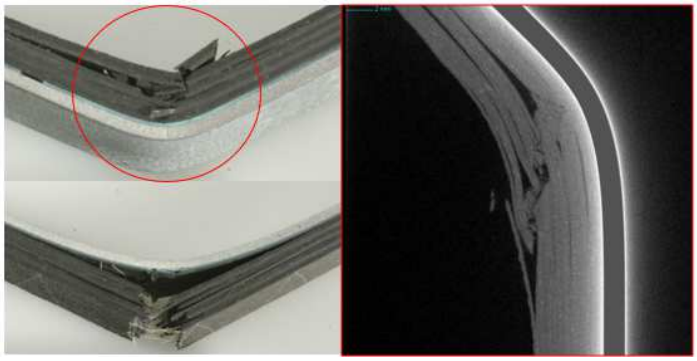

Figure 14: Failure modes of 3-point-bending specimens with respect to the loading direction

While the major amount of energy is dissipated in the fracturing FRP laminate, the steel phase has a supporting and stabilizing effect during the specimen's failure resulting in a hybrid mechanism. Next to a comparably high *SEA*, this hybrid mechanism results in a relatively homogeneous force-displacement-curve which is of vital importance for energy absorbing structures in crash applications. Figure 15 shows the force-displacement-plots of two hybrid specimens tested with different loading directions.

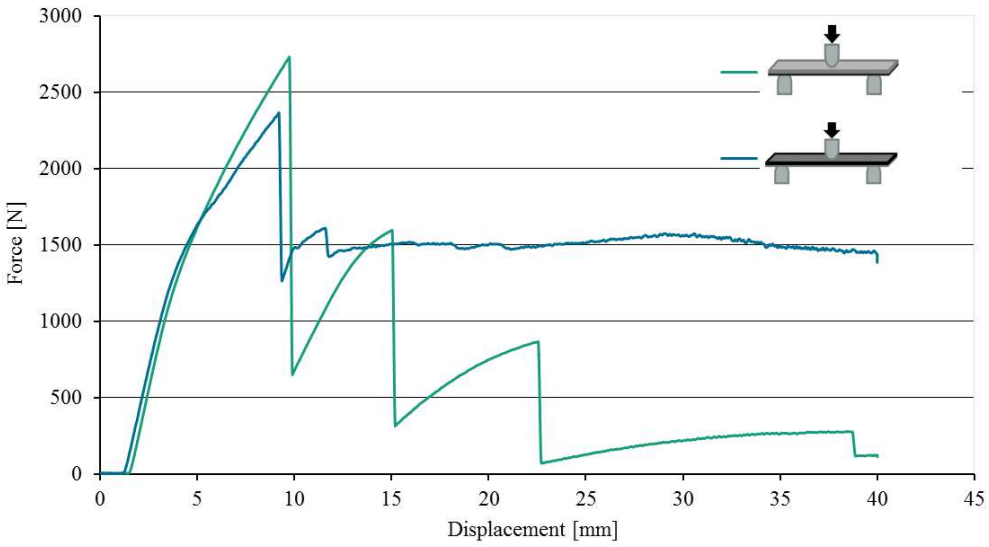

Figure 15: Force-displacement-plots of hybrid specimens with different loading directions
Parameters: HCT, CFRP, 16 plies, [0°/90°]-layup

With FRP facing the fin (blue curve) the force increases with a rising deflection until a first laminate fracture takes place. After that, the load remains on a comparably constant and high level until the end of the experiment.

5 SUMMARY

Hybrid material systems consisting of glass and carbon fiber reinforced plastics and steel have been tested under tension and 3-point-bending. The experiments with strip-shaped specimens generally confirm anticipated effects on the base of analytic and rule-of-mixture calculations. Although the stiffness and strength show a clear dependence on the fiber orientation, with the given steel to composite ratios from 1:2 to 1:4 the specimens' loading and failure behavior is dominated by the steel and its characteristics. The structural adhesive generally shows a good performance and does not cause any systematic premature specimen failure. Interestingly, the fiber type predominantly shows a minor effect on the mechanical characteristics. Considering the distinctly higher prices for carbon fibers compared to glass fibers, this could be crucial concerning future mid or high volume applications of hybrid material systems. The exact (micro-) mechanical backgrounds of the hybrid mechanisms presented for tension and 3-point-bending tests require some in-depth investigation through further experimental and simulation analyses. Nevertheless, a distinct extension of the maximum strain is observed for both composites (28 % CFRP, 48 % GFRP) and (press hardened) steel (23 %) when joined in a hybrid specimen and tested under tensile loads. This effect is a result of internally induced lateral stresses that cause an extension of longitudinal maximum strain.

In 3-point-bending, a higher *SEA* for hybrid specimens with pressure loaded composites (facing the fin) compared to tension loaded composites (facing the supports) is observed. The increase of 26 % (for [0°/90°]-layups) is caused by the interaction of both constituent materials. With the steel phase having a stabilizing and supporting effect, the FRP was simultaneously being subject to a multitude of failure mechanisms such as fiber fracture and delamination.

Next to a deeper verification of the presented results – also in the dynamic loading range - further research is focused on numerical simulation techniques for hybrid materials and an experimental investigation on transferring the findings from the coupon tests to the crash component level.

ACKNOWLEDGEMENTS

The authors would like to express their gratitude to their colleagues at Fraunhofer Ernst-Mach-Institute (EMI) for their support during testing and evaluation as well as for valuable discussions. Also, the authors would like to thank their partners at Salzgitter Mannesmann Forschung GmbH and BMW Group for their trusting support.

REFERENCES

[1] European Union. 2009. *Regulation (EC) No 443/2009 of the European Parliament and the Council of 23 April 2009*.

[2] Haldenwanger, H.-G. 1997. *Zum Einsatz alternativer Werkstoffe und Verfahren im konzeptionellen Leichtbau von PKW-Rohkarosserien*. Dissertation, Technische Universität Dresden.

[3] Elend, L.-E. and Durst, K. G. 2011. *Wettbewerb der Leichtbauwerkstoffe*. Automotive Forum, Ingolstadt.

[4] Karbe, E. 2013. *Leichtbau im Automobilbau*. i2b meet-up "Leichtbau als Schlüsseltechnologie für Bremen", Bremen.

[5] Koch, B., Knözinger, G., Pleschke, T., and Wolf, H. J. 1999. Hybrid-Frontend als Strukturbauteil. *Kunststoffe* 89, 3, 82–86.

[6] Grasser, S. 2009. *Composite-Metall-Hybridstrukturen unter Berücksichtigung großserientauglicher Ferigungsprozesse*. Symposium Material Innovativ, Ansbach.

[7] Hufenbach, W., Werner, J., and Kiele, J. 2013. Elektromobilität in Ultraleichtbauweise. *ATZ Extra* 18, 2, 42–46.

[8] Feraboli, P., Deleo, F., Wade, B., Rassaian, M., Higgins, M., Byar, A., Reggiani, M., Bonfatti, A., DeOto, L., and Masini, A. 2010. Predictive modeling of an energy-absorbing sandwich structural concept using the building block approach. *Composites Part A: Applied Science and Manufacturing* 41, 6, 774–786.
[9] Frantz, M., Lauter, C., and Tröster, T. 2011. *Advanced manufacturing technologies for automotive structures in multi-material design consisting of high-strength steels and cfrp*, University of Paderborn.
[10] Eckstein, L., Ickert, L., Goede, M., and Dölle, N. 2011. Leichtbau-Bodengruppe mit Verstärkungen aus CFK und GFK. *ATZ (ATZ - Automobiltechnische Zeitschrift)* 113, 4, 256–261.
[11] Costas, M., Díaz, J., Romera, L., Hernández, S., and Tielas, A. 2013. Static and dynamic axial crushing analysis of car frontal impact hybrid absorbers. *International Journal of Impact Engineering* 62, 166–181.
[12] Wang, X. G., Bloch, J. A., and Cesari, D. 1992. Static and dynamic axial crushing of externally reinforced tubes. *ARCHIVE: Proceedings of the Institution of Mechanical Engineers, Part C: Journal of Mechanical Engineering Science 1989-1996 (vols 203-210)* 206, 53, 355–360.
[13] Bouchet, J., Jacquelin, E., and Hamelin, P. 2002. Dynamic axial crushing of combined composite aluminum tube: the role of both reinforcement and surface treatments. *Composite Structures* 56, 1, 87–96.
[14] Shin, K. C., Lee, J. J., Kim, K. H., Song, M. C., and Huh, J. S. 2002. Axial crush and bending collapse of an aluminum/GFRP hybrid square tube and its energy absorption capability. *Composite Structures* 57, 1-4, 279–287.
[15] Kim, H. C., Shin, D. K., Lee, J. J., and Kwon, J. B. 2014. Crashworthiness of aluminum/CFRP square hollow section beam under axial impact loading for crash box application. *Composite Structures* 112, 1–10.
[16] Bambach, M. and Elchalakani, M. 2007. Plastic mechanism analysis of steel SHS strengthened with CFRP under large axial deformation. *Thin-Walled Structures* 45, 2, 159–170.
[17] Bambach, M., Elchalakani, M., and Zhao, X. 2009. Composite steel–CFRP SHS tubes under axial impact. *Composite Structures* 87, 3, 282–292.
[18] Bambach, M., Jama, H., and Elchalakani, M. 2009. Axial capacity and design of thin-walled steel SHS strengthened with CFRP. *Thin-Walled Structures* 47, 10, 1112–1121.
[19] Bambach, M., Jama, H., and Elchalakani, M. 2009. Static and dynamic axial crushing of spot-welded thin-walled composite steel–CFRP square tubes. *International Journal of Impact Engineering* 36, 9, 1083–1094.
[20] Bambach, M. 2010. Axial capacity and crushing of thin-walled metal, fibre–epoxy and composite metal–fibre tubes. *Thin-Walled Structures* 48, 6, 440–452.
[21] Bambach, M. 2010. Axial capacity and crushing behavior of metal–fiber square tubes – Steel, stainless steel and aluminum with CFRP. *Composites Part B: Engineering* 41, 7, 550–559.
[22] Bambach, M. R. 2013. Fibre composite strengthening of thin-walled steel vehicle crush tubes for frontal collision energy absorption. *Thin-Walled Structures* 66, 15–22.
[23] Mamalis, A., Manolakos, D., Ioannidis, M., and Papapostolou, D. 2005. On the response of thin-walled CFRP composite tubular components subjected to static and dynamic axial compressive loading: experimental. *Composite Structures* 69, 4, 407–420.
[24] Lukaszewicz, D. H.-J. A. 2013. Automotive Composite Structures for Crashworthiness. In *Advanced Composite Materials for Automotive Applications*, A. Elmarakbi, Ed. John Wiley & Sons Ltd, Chichester, UK, 99–127.
[25] Sadighi, M., Alderliesten, R. C., and Benedictus, R. 2012. Impact resistance of fiber-metal laminates: A review. *International Journal of Impact Engineering* 49, 77–90.
[26] Uriayer, F. A. J. The new Steel-CFRP composite specimen (CFRP laminates sandwiched between two steel strips) and its behaviour under uniaxial tension. In *Internatinal Journal of Civil Engineering*, 249–258.
[27] Mildner, C. 2013. *Numerische und experimentelle Untersuchungen des Crashverhaltens von FVK-verstärkten Metallstrukturbauteilen*. Dissertation, Technische Universität München.
[28] Salzgitter Flachstahl. 2009. *HCT600XD (HC340XD*)*. Mehrphasenstähle zum Kaltumformen - Dualphasenstähle, Salzgitter.

[29] Salzgitter Flachstahl. 2010. *22MnB5*. Borlegierte Vergütungsstähle, Salzgitter.
[30] SGL Group. 2014. *PREDO PR-UD CS 300/600 FT102 38*. Technical Data Sheet, Willich.
[31] SGL Group. 2014. *PREDO PR-UD EST 300/300 FT102 35*. Technical Data Sheet, Wilich.
[32] SGL Group. 2014. *Epoxid-Prepreg FT102*. Produkt Information Epoxid-Prepreg FT102, Willich.
[33] Dow Automotive AG. 2003. *Betamate 2096*. Technisches Datenblatt.
[34] Engel, S., Boegle, C., Majamaeki, J., Lukaszewicz, D. H.-J. A., and Moeller, F. 2012. Experimental inverstigation of composite structures during dynamic impact. In *ECCM15 - 15th European Conference on Composite Mateials*.
[35] GOM mbH. 2009. *Aramis*. *User Manual - Software*, Braunschweig.
[36] DIN - Deutsches Institut für Normung e.V. 1997. *Kunststoffe - Bestimmung der Zugeigenschaften*. Beuth Verlag, Berlin, DIN EN ISO 527-4.
[37] DIN - Deutsches Institut für Normung e.V. 2011. *Faserverstärkte Kunststoffe - Bestimmung der Biegeeigenschaften*. Beuth Verlag, Berlin, DIN EN ISO 14125.
[38] Verein Deutscher Eisenhüttenleute (Hrsg.). 1984. *Werkstoffkunde Stahl*. *Band 1: Grundlagen*. Springer Berlin Heidelberg, Berlin, Heidelberg.
[39] Kumazawa, H. and Takatoya, T. 2009. Biaxial strength investigation of CFRP composite laminates by using cruciform specimens. In *The 17th International Conference on Composite Materials*.